

THE OFFICIAL MAGAZINE OF THE OCEANOGRAPHY SOCIETY

Oceanography

CITATION

Meselhe, E., D. Roelvink, C. Wackerman, F. Xing, and V.Q. Thanh. 2017. Modeling the process response of coastal and deltaic systems to human and global changes: Focus on the Mekong system. *Oceanography* 30(3):84–97, <https://doi.org/10.5670/oceanog.2017.317>.

DOI

<https://doi.org/10.5670/oceanog.2017.317>

COPYRIGHT

This article has been published in *Oceanography*, Volume 30, Number 3, a quarterly journal of The Oceanography Society. Copyright 2017 by The Oceanography Society. All rights reserved.

USAGE

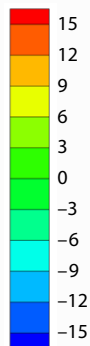
Permission is granted to copy this article for use in teaching and research. Republication, systematic reproduction, or collective redistribution of any portion of this article by photocopy machine, reposting, or other means is permitted only with the approval of The Oceanography Society. Send all correspondence to: info@tos.org or The Oceanography Society, PO Box 1931, Rockville, MD 20849-1931, USA.

Modeling the Process Response of Coastal and Deltaic Systems to Human and Global Changes

FOCUS ON THE MEKONG SYSTEM

By Ehab Meselhe,
Dano Roelvink, Christopher Wackerman,
Fei Xing, and Vo Quoc Thanh

Elevation (m)



ABSTRACT. Coastal zones are constantly changing in response to meteorological and hydrodynamic conditions. Water levels associated with storms, coupled with wind-driven waves, can significantly reshape coastal and deltaic geomorphology. Conversely, coastal wetlands attenuate waves, surge, and currents. These interactions have profound implications for ecosystem function and human infrastructure. This article discusses how predictive numerical models and remote-sensing techniques can advance understanding of the dominant process response (and feedbacks) of coastal and deltaic systems to a wide range of natural and anthropogenic changes. Remote-sensing techniques can provide valuable information at large spatial scales (10^1 – 10^3 km²) and at temporal scales ranging from days to decades that can be used to parameterize and validate numerical models, especially in regions such as the Mekong Delta where in situ data are sparse. Applications to the Mekong Delta system illuminate how modeling tools can reliably predict and describe system dynamics. Numerical modeling supported by remote-sensing information is an effective approach for evaluating and examining restoration and protection strategies, and for ameliorating the effects of climate change, natural hazards, and anthropogenic alterations to coastal ecosystems and human communities.

INTRODUCTION AND BACKGROUND

Coastal regions are among the most productive and dynamic ecogeomorphic systems in the world. With a long history of human reliance on their natural resources for food, commerce, recreation, protection, and cultural identity, habitation of coastal areas is still rapidly increasing (Dennison, 2008). It has been estimated that 10% of the global population lives in coastal areas less than 10 m above sea level (McGranahan et al., 2007), and 25% will live in the flood-prone coastal zone by 2050 (Aerts et al., 2014). Immediate threats come from the extreme water levels associated with storms that are amplified by sea level rise (SLR) and by subsidence caused by both natural and anthropogenic factors. This is especially true for deltaic and estuarine systems.

There is a critical need to better understand the valuable coastal and deltaic systems, but these environments are challenging to model because their characteristics vary greatly across the globe. Morphodynamic studies supported by observations highlight the wide variability in fluvial-ocean exchange across deltaic and coastal systems worldwide

(Kim et al., 2009; Paola et al., 2011; Giosan et al., 2014; Smith et al., 2015). For instance, the lower Mississippi River (annual average discharge of 530 billion cubic meters, average tidal range at the river mouth of 0.3 m; Allison and Neill, 2002; Rabouille et al., 2008) is predominantly governed by fluvial discharge and man-made engineering structures that have created a freshwater-dominated and non-reversing tidal channel that carries a large amount of sediment to the shelf, but whose low-discharge period is dominated by highly stratified estuarine intrusion (Wright and Coleman, 1974; Allison et al., 2012). Conversely, in the Ganges-Brahmaputra Delta (annual average discharge of 993 billion cubic meters, average tidal range at the river mouth of 3.6 m; Jian et al., 2009; Walsh and Nittrouer, 2009), tides are the dominant mechanism of sediment exchange with the ocean. In tide-dominated deltaic systems, sediment in the river channels is redistributed by tidal currents, with net import into the river system through flood-dominated distributaries and net export to the ocean through ebb-dominated distributaries (Barua, 1990). In many of these low-gradient deltaic systems (e.g., Bay of

Bengal), saltwater typically penetrates as far as 100 km inland during the low-flow season (Allison, 1998). The lower Yangtze channel (annual average discharge of 925 billion cubic meters, average tidal range at the river mouth of 3.4 m; Hori et al., 2001, 2002; Rabouille et al., 2008) is also governed by tides, but is highly influenced by the seasonal variations of fluvial discharge. During the low-flow season, there is significant saltwater intrusion. Seasonal variation is likely to influence sediment transport patterns (P. Xue et al., 2009; Wu et al., 2010; Xu et al., 2012;).

This article provides an overview of numerical model predictive tools that can be used to further understanding of challenges facing deltaic and coastal systems. These numerical tools, once validated, can be used to understand how coastal systems respond to anthropogenic and natural alterations of the environmental drivers. We also summarize remote-sensing techniques and how they can be used to parameterize and validate these numerical models by providing large-spatial-scale information (e.g., chlorophyll, suspended sediment, and temperature) over a range of temporal scales. The Mekong system in Vietnam is presented as an example to illustrate the utility of numerical models and remote-sensing tools.

THE MEKONG DELTAIC SYSTEM

The lower Mekong River (annual average discharge of 470 billion cubic meters, average tidal range at the river mouth of 2.2 m; Thuy, 1979; Milliman and Syvitski, 1992), which flows through the third largest delta system in the world and provides homes for 18 million Vietnamese, is dominated by tides and seasonal variations of fluvial discharge (Figure 1). With a total length of 4,750 km and a drainage area of 832,000 km² (Z. Xue et al., 2011), the Mekong River has the seventh largest water discharge and eleventh largest sediment discharge worldwide.

Estimates of the annual sediment load for the Mekong River vary significantly from 40 to 160 million tons (Nowacki et al., 2015: 40 Mt yr⁻¹; Lu et al., 2014: 50–91 Mt yr⁻¹; Milliman and Farnsworth, 2013: 110 Mt yr⁻¹; Walling, 2008: 160 Mt yr⁻¹). Milliman and Farnsworth (2013) estimated that the dissolved sediment load is ~ 60 Mt yr⁻¹. The decreased freshwater flow in the lower Mekong channel in the low-flow season intensifies saltwater intrusion (the distance upstream reached by saltwater on the incoming tide), which penetrates ~ 45 km upstream of the river mouth (Gagliano and McIntire, 1968) and threatens domestic, industrial, and agricultural freshwater usage. Further, the lower Mekong River system is significantly subsiding, sea level is rising, and the coast is eroding, all of which are expected to threaten the future sustainability of the river and delta system. Groundwater extraction results in high sediment-layer compaction rates (1.68 cm yr⁻¹), which will lead to an estimated 88 cm of land subsidence by 2050 (Erban et al., 2014). Eustatic sea level at the lower Mekong River is predicted to rise by 28 cm to 33 cm by 2050 and 65 cm to 100 cm by 2100 (MONRE, 2009), causing one to two million residents to be at

risk by 2050 (Ericson et al., 2006; Carew-Reid, 2008; McSweeney et al., 2010). New dams under construction upstream are expected to trap more than 90% of sediment that otherwise would be transported to the lower river system (Kondolf et al., 2015; Manh et al., 2015), potentially intensifying the negative impact of land subsidence and bank erosion. On top of this, (largely illegal) sand mining has been taking place on a massive scale, estimated as great as 28 million m³ yr⁻¹ (Manh et al., 2015; Anthony et al., 2015). These changes will significantly influence the dynamics of the lower Mekong River and further impact the evolution of the Mekong Delta.

Early investigations have used numerical models to study the Mekong system. For example, Nguyen et al. (2008) estimated the freshwater budget between the lower Mekong branches with a saltwater intrusion model that showed the general freshwater distribution patterns in the multiple channels of the lower Mekong River system. More data and refinements are needed to improve the accuracy of this approach. Recent field observations gathered in the Dinh An subchannel, the dominant segment of the lower Song Hau distributary channel, show the

hydrodynamics and sediment-transport patterns in both the high- and low-flow seasons (Wolanski et al., 1998). These observations were also used to estimate the yearly sediment yield of the Mekong River (Nowacki et al., 2015). However, due to the difficulties and cost of field campaigns, the observations were very limited. Their short duration does not accurately capture the temporal variability of the sediment transport and ultimately leads to uncertainties in the estimates. Former studies investigated the fine-sediment transport in the Dinh An subchannel (Wolanski et al., 1998; Hein et al., 2013), while sand movement in the system, specifically in the Tran De subchannel (also part of the Song Hau channel) and the interactions between the two subchannels, are still relatively unquantified. It has been argued that the importance of Mekong River sand dynamics have been underestimated, and Nowacki et al. (2015) observed the substrate of the lower Song Hau subchannels to be dominated by sand. Therefore, sand dynamics may play an important role in controlling the evolution of the lower Song Hau channel (Bravard et al., 2014). Additional details about the system dynamics can be found in Xing et al. (in press).

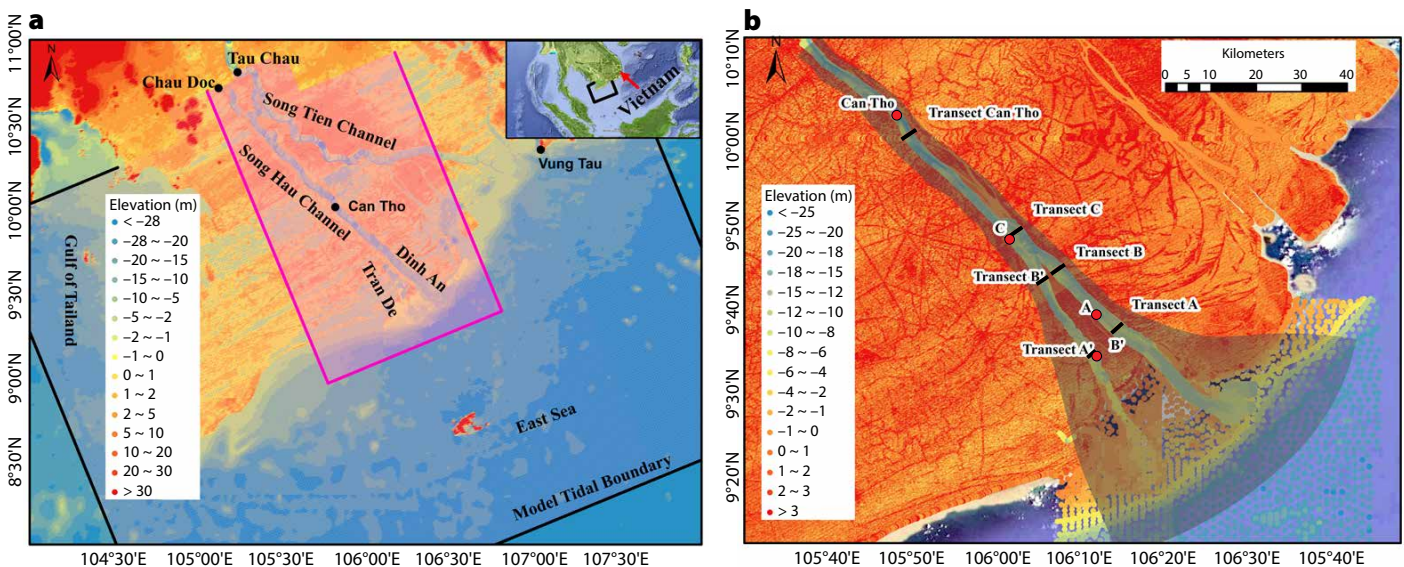


FIGURE 1. General (a) and detailed (b) maps of the Song Hau channel in the Mekong River delta, Vietnam. In (a), the black and magenta lines designate the nested two-dimensional model grids. The magenta line shows the domain decomposition boundary between the fine grid inner domain and the coarse grid outer domain. The black circles show the two stations at upstream river boundaries (Chau Doc and Tan Chau), Can Tho monitoring station, and a tide station at Vung Tau. In (b), the shaded area shows the high-resolution channel model grid, and the red circles and black lines show the observational stations and transects, respectively, during the 2014 and 2015 field campaigns. From Xing et al. (in press)

ANALYSIS AND PREDICTION TOOLS

Physically Based Numerical Models

Traditional divides among research disciplines have hindered understanding of large-scale coastal and deltaic ecosystems. Integrated modeling approaches are needed to interface the ecology, geomorphology, and engineering disciplines. Such interdisciplinary modeling techniques would further the understanding of long-term landscape dynamics that result from either “fair-weather” conditions or extreme events that last hours or days. However, the range of process-relevant scales involved is formidable. Time scales extend from turbulence-driven sediment fluxes to decadal accumulations of sediment. Spatial scales extend from narrow topographic features like bedforms to large spans of vegetated tidal land. At the fundamental process level, an understanding of the interactions and feedbacks that drive landscape change and dynamics over the broad range of scales will potentially allow these computational tools to aid in management of sustainable and resilient coastal and deltaic ecosystems (Meselhe et al., 2015).

Numerical models have been used extensively to study riverine, deltaic, and coastal systems. Models range in complexity from simple planning models to high-resolution dynamic models. It is beyond the scope and intent of this article to survey the various modeling approaches. Rather, the focus will be on a publicly available open source code and a widely applied morphodynamic modeling system, Delft3D (Sutherland et al., 2003; Edmonds and Slingerland, 2007, 2010; Caldwell and Edmonds, 2014; Vinh et al., 2016; Yuill et al., 2015, 2016; Gaweesh and Meselhe, 2016; Meselhe et al., 2016). Delft3D is a three-dimensional modeling system (that can also be applied as depth-averaged) that consists of integrated modules to simulate fluid flow, wave generation and propagation, sediment transport, and morphological changes (Lesser et al., 2004;

Deltares, 2011). The Delft3D hydrodynamic and morphodynamic modules are fully coupled computationally where the evolving bathymetry (caused by deposition and erosion) interacts with and influences the flow field and vice versa. This modeling tool allows for long-term simulations of morphological evolution (i.e., years to decades) through the use of numerical acceleration techniques (Lesser et al., 2004; Deltares, 2011). The Delft3D FLOW module has a finite difference solution of the three-dimensional shallow-water equations and the $k-\epsilon$ turbulence-closure model to compute flow characteristics under the hydrostatic pressure assumption. A recent update to the model includes an unstructured grid capability that significantly facilitates the ability of the model to efficiently capture complex geometries of deltaic and coastal systems. The model includes sediment transport (both suspended and bedload) and morphologic processes (e.g., deltaic growth and decay, channel bifurcations, bank-line migration).

Satellite-Based Remote-Sensing Tools

The models discussed in this paper generate outputs over large spatial and temporal scales, which often make validation of model output difficult. In situ observations of predicted quantities such as suspended sediment concentrations (SSC) or water velocity can provide high-quality validation data, but only at one location and only for a limited time, usually days to weeks. These data cannot help with validation across the river system (where parameters have great spatial variability) or over long temporal scales (seasons to decades). Satellite-based remote-sensing systems can potentially address this issue. There are sensors that have a field of view that can cover an entire river system, such as the Mekong Delta (Figure 2). Although satellite systems cannot generate imagery with time sampling on the scale of in situ measurements (minutes to hours), they can generate images on temporal scales consistent with changes in river dynamics

(days to weeks), and can generate time series that span months and even decades. Thus, satellite-based remote sensing has the spatial and temporal capabilities to provide significant model validation data sets and long-term trends.

There are other limits on remote-sensing effectiveness. The optical wavelengths used by multispectral image (MSI) sensors cannot penetrate clouds. Thus, useful, cloud-free imagery can require longer temporal spacing that depends on local weather. In contrast, synthetic aperture radar (SAR) sensors use microwave radiation that can see through clouds, so weather does not affect their temporal cycles. However, SAR tends to image turbid rivers as constant dark features in contrast to the range of visible features apparent in MSI imagery. Perhaps most importantly, remote-sensing images need to be translated into estimates of quantities (e.g., sediment concentration, surface temperature) that can be used to validate numerical models for these riverine and coastal systems.

A conversion algorithm is needed to translate the numbers that can be extracted from remote-sensing imagery and generate an estimate for specific quantities of interest, such as sediment load or river flow, that can be directly compared to numerical model outputs. MSI sensors have proved particularly useful in this regard. Multiple validated algorithms have been developed to translate MSI data collected at different wavelengths of light (optical bandwidth) into various water properties such as concentrations of chlorophyll and particulate matter, attenuation coefficient, and sea surface temperature (<https://oceancolor.gsfc.nasa.gov>). The MSI bands are sensitive to the suspended sediment in the portion of the water column over which the radiation will penetrate. For sediment levels typical of the Mekong Delta ($\sim 0.1 \text{ g L}^{-1}$), this is approximately the upper 2 m of the water column (Stumpf and Pennock, 1989). MSI images will thus show upper-layer sediment patterns as variations of brightness within optical



FIGURE 2. Example of remote-sensing images that can cover an entire river system. This Landsat multispectral image (MSI) has been turned into a false-color image using the sensor's blue, green, and red bands. From Wackerman et al. (in press)

bands. Figure 2 clearly shows the plumes emanating from of the Dinh An and Tran De channels into the ocean.

Much work has been done on generating quantitative estimates of SSC from MSI remote-sensing imagery, with some of the early studies estimating SSC in freshwater and estuarine environments (Ritchie et al., 1976; Holyer, 1978). Numerous studies over a range of areas and approaches have since been published (e.g., Curran and Novo, 1988; Mertes et al., 1993; Bowers and Binding, 2006; Pavelsky and Smith, 2009; Long and Pavelsky, 2013; Park and Latrubesse, 2014). Generally, theoretical and empirical studies show that optical bands are highly correlated with SSC (Holyer, 1978; Kirk, 1994), particularly in the red (wavelength range of 610–700 nm) and near-infrared (wavelength range of

700–1,000 nm) bands. The relationship between SSC and reflectivity is generally linear in optical bands (blue, green, and red) if SSC is within the range of 0–50 mg L⁻¹ (Munday and Alfoldi, 1979; Ritchie et al., 2003; Kilham and Roberts, 2011; Kilham et al., 2012). There is an exponential relationship for greater values of SSC (Curran and Novo, 1988; Holyer, 1978), particularly in the near-infrared bands (NIR), though this becomes uncorrelated for lesser SSC values (< ~50–70 mg L⁻¹).

Regression models are a general class of approaches developed to estimate SSC using parameters that can be extracted from remote-sensing imagery. Such models regress to the SSC on the reflectivity values from various wavelength bands, fitting to the reflectivity values themselves and/or to ratios of the reflectivity values.

The fits are done either using the SSC values (a linear model) or using the logarithm of SSC (an exponential model) and generally are of linear or second order, with linear being the most common. The models are generated using a specific set of in situ observations (i.e., collected at a specific location and time) and for a specific remote-sensing system, and thus generally are only considered applicable to that specific data set (Doxaran et al., 2002, 2003, 2009; Pavelsky and Smith, 2009; Wang and Lu, 2010; Miller et al., 2011; Long and Pavelsky, 2013; Sravanthi et al., 2013; Park and Latrubesse, 2014).

Using these approaches to calibrate the data, MSI remote-sensing imagery is capable of providing SSC estimates for the top section of the water column over periods of weeks to years to decades at spatial scales covering large riverine and coastal systems. Such estimates can be directly compared to numerical model outputs for calibration or validation, or to determine model input parameters. In addition, remote-sensing-generated SSC trends, or related metrics such as coastal erosion or growth, can be used to characterize system changes over the long term. It is important to note, however, that due to the temporal sampling of remote-sensing imagery, diurnal or episodic events can be undersampled or missed entirely. Thus, remote-sensing data are useful in providing longer-term trends of riverine properties, for example, monthly averages over spatial and temporal extents that typically cannot be measured with in situ devices.

MEKONG DELTA EXAMPLES

Applications of Numerical Models

A depth-averaged (two-dimensional) Delft3D model was developed to study seasonal to annual channel morphodynamics (Figure 1). The model includes two nested domains, with the inner domain covering the Song Hau distributary and adjacent floodplain, while the outer domain covers the Song Tien distributary, the surrounding flood plains, the adjacent East Sea (also known

as South China Sea) and the Gulf of Thailand (Figure 1a).

In addition to the models described above, high-resolution channel models, using both two- and three-dimensional approaches, were developed for the lower Song Hau channel. The models were used to study the detailed hydrodynamics and sand dynamics of high- and low-flow

seasons, as well as the spring-neap and flood-ebb tidal cycles of the lower Song Hau channel. The models were validated against the March 2015 (low river discharge) and September 2014 (high discharge) field campaigns described in Allison et al. (in press). The models were then applied to examine seasonal flow and sediment dynamics. Figure 3 shows

a sample of the model output. Figure 3b compares the predicted and measured flow discharge during neap and spring tides at the locations identified in Figure 1. Figure 3a,c shows the vertical flow structure along several observational transects within the bidirectional flow zone. The seaward flow (ebb tide) had a greater velocity than the landward flow

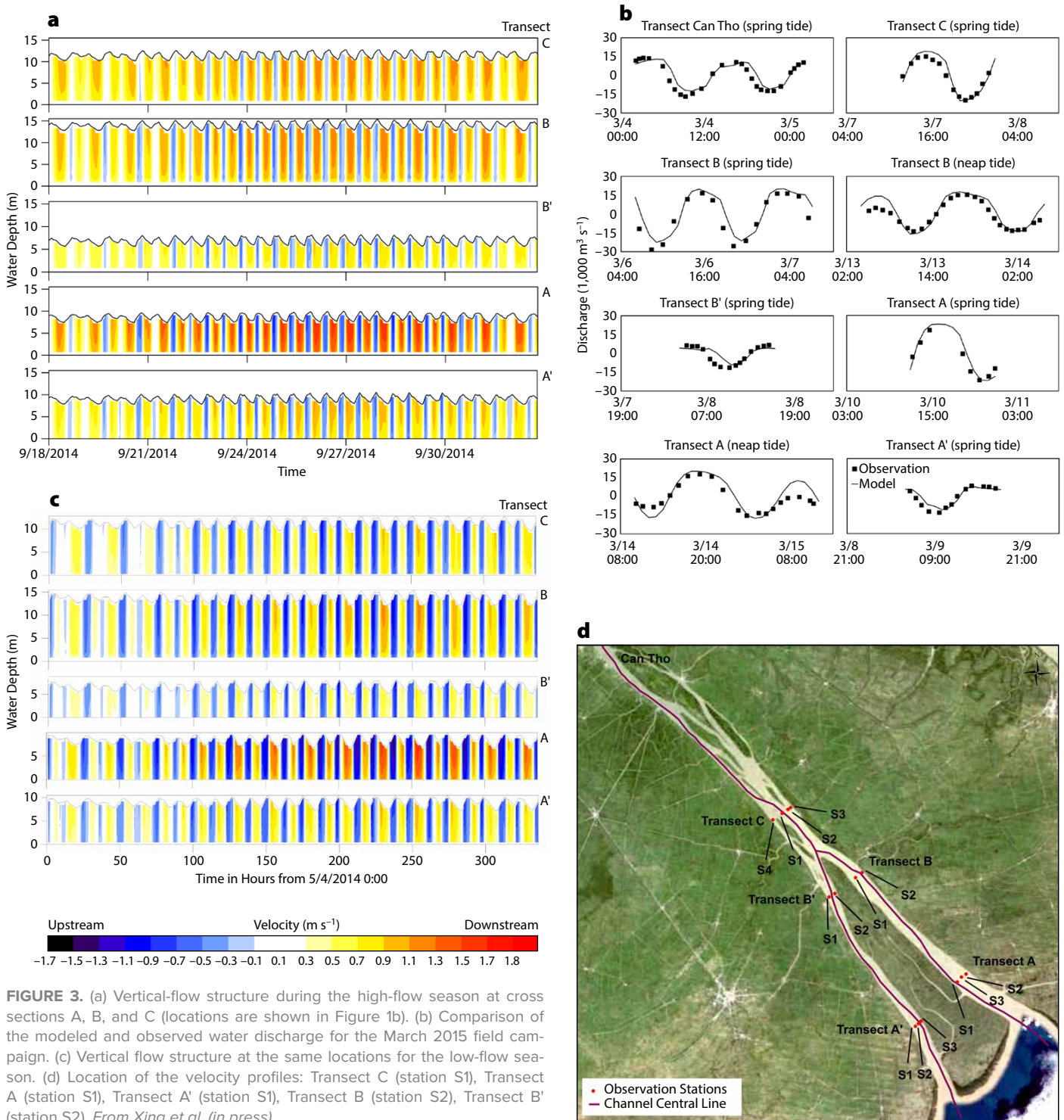


FIGURE 3. (a) Vertical-flow structure during the high-flow season at cross sections A, B, and C (locations are shown in Figure 1b). (b) Comparison of the modeled and observed water discharge for the March 2015 field campaign. (c) Vertical flow structure at the same locations for the low-flow season. (d) Location of the velocity profiles: Transect C (station S1), Transect A (station S1), Transect A' (station S1), Transect B (station S2), Transect B' (station S2). From Xing et al. (in press)

(flood tide), and both maximum seaward and landward flow velocities occurred during spring tides.

In a parallel effort, Thanh et al. (in press) use a suite of Delft3D models for the Mekong Delta system, including a depth-averaged, delta-wide, unstructured-grid model and a three-dimensional model of the main channels and the shelf. Comparison of in situ measurements and remote-sensing data with the model demonstrates that the model is capable of qualitatively simulating sediment dynamics on the delta shelf. These simulations indicate that a substantial amount of sediment delivered by the Mekong River is deposited in front of the river mouths during the flood season and resuspended in the dry season. These processes were confirmed by observations (Nittrouer et al., 2017, in this issue;

Ogston et al., in press).

A sensitivity analysis demonstrated that waves, salinity, and sediment processes strongly influence suspended sediment distribution and transport on the shelf. In particular, wave effects play an essential role in sediment resuspension. Figure 4a shows the horizontal and vertical sediment distributions just after the peak of ebb, September 23, 2014, at 6AM UTC. Horizontally, the model shows a spatial pattern quite similar to that depicted by the MODIS-Aqua-derived satellite image at the same time, with the typical double-pronged plume emanating from the Song Hau (also referred to as the Bassac) mouth. The vertical distribution along the channel axis of the Song Hau shows a typical situation, where a surface freshwater plume carries fine sediments. The cause of this pattern is confirmed by examining

the surface salinity along the Song Hau channel axis (Figure 4b).

The overall delta model was run for two years and the three-dimensional model for approximately one year. Encouragingly, the models showed the well-documented behavior of a northeast-directed plume in August–October during high discharge, with sediment deposited on the delta fronts and beyond. Subsequently, this sediment is resuspended during spring tides and wave events and transported toward the southwest during the northeast monsoon. The model, which contained both sand and mud fractions, is currently being used to establish a near-equilibrium near-surface bed composition through long-term (~decadal) simulations.

As shown above, numerical models provide valuable spatial and

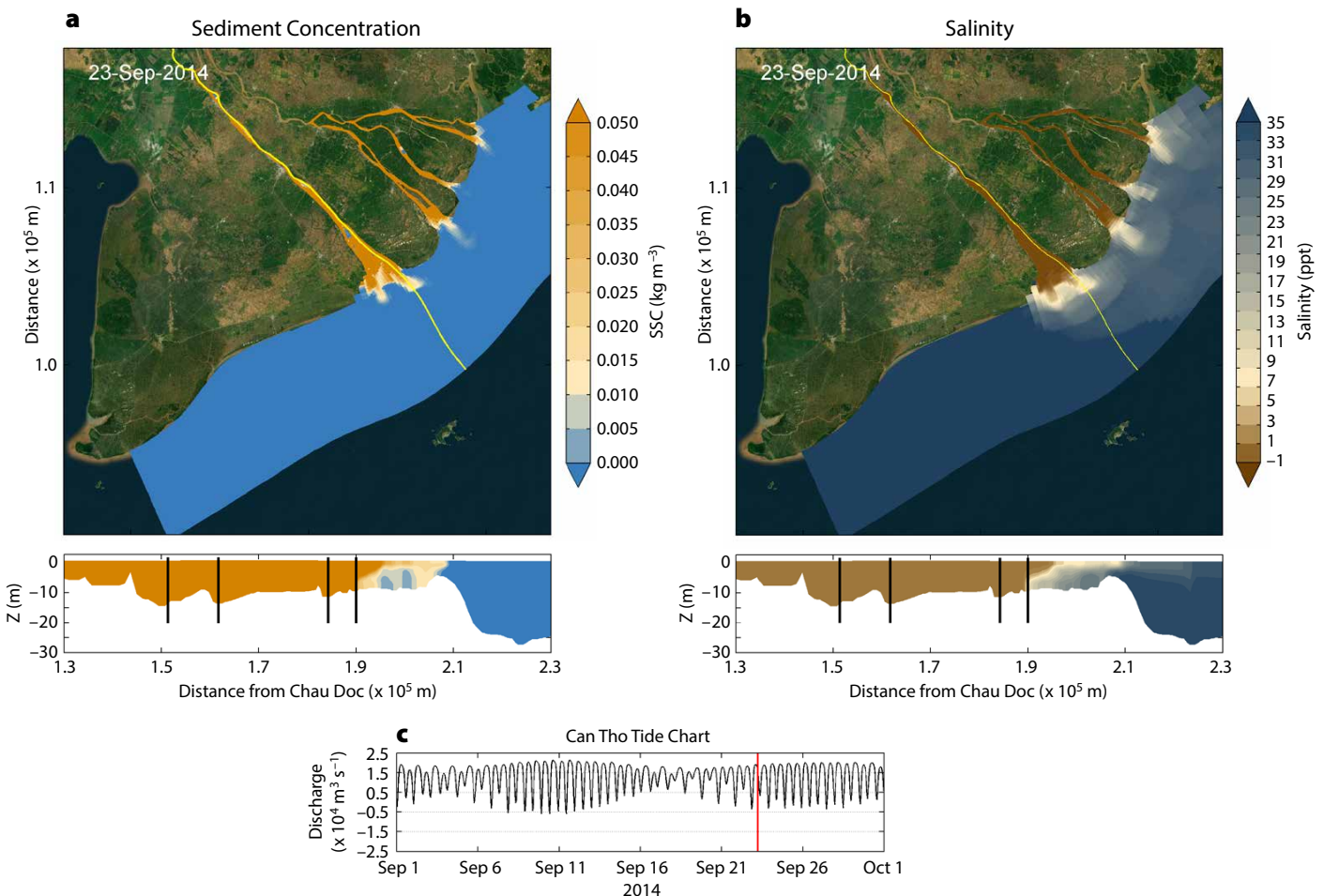


FIGURE 4. (a) Sediment and (b) salinity distribution (vertical and horizontal) near the mouth of the Song Hau (Bassac) channel. The four vertical black solid lines indicate (from right to left) the tip of the island of Cu Lao Dung and sections A through C (locations of sections A through C are shown in Figure 1). It should be noted that the island is permanently dry; the concentrations shown on top of the island are simply remnants of the initial conditions. (c) The tide record was collected at the city of Can Tho, and the time of the sediment and salinity observations in 2014 are shown by the vertical red line.

temporal information on system dynamics. However, further tool development is needed to improve the models' ability to capture the complex processes governing coastal and deltaic systems. Additionally, more data are needed to adequately calibrate and validate these numerical models.

Applications of Remote-Sensing Tools

To make use of the available remote-sensing databases for the Mekong deltaic system, the first step is to calibrate the imagery. Two in situ observation campaigns were conducted, one in September 2014 during high-flow conditions and the other in March 2015 during low-flow conditions (Ogston et al., in press). During the campaigns, in situ measurements of SSC as a function of water depth were collected from ships using integrated optical backscatter sensors as well as water samples for calibrating the optical data (Eidam et al., in press; McLachlan et al., in press). MSI observations from Landsat, MODIS, and RapidEye sensors were also collected September 2014 through March 2015 and converted to surface reflectance in the blue, green, red, and near-infrared NIR bands after masking clouds and land using standard algorithms (Zhu and Woodcock, 2012). The remote-sensing imagery was then correlated with in situ observations of SSC. Whenever an in situ observation was made in concert with a cloud-free image

field of view, and within ± 30 minutes of image collection, it was considered coincident with the remote-sensing data. For each of these, the SSC values from the region in the water column where remote-sensing radiation is expected to penetrate (~ 2 m) were averaged to generate ground-truth SSC values for comparison to the remote-sensing surface reflectance data. The mean and standard deviation of the remote-sensing surface reflectances were then calculated over a $1.5 \text{ km} \times 1.5 \text{ km}$ window (3×3 samples) for MODIS imagery, a $150 \text{ m} \times 150 \text{ m}$ window (5×5 samples) for Landsat imagery, and a $30 \text{ m} \times 30 \text{ m}$ window (5×5 samples) for RapidEye imagery, centered over the location of the coincident in situ SSC observation. Window sizes were chosen to provide the best spatial resolution of the resulting SSC estimates with reasonable suppression of image noise. Each window was manually examined to make sure that there were no land responses within the window; if there was, the window was shifted slightly to remove them. From the resulting test data, the goal was to develop one algorithm that could be used to estimate SSC from these sensors over the Mekong Delta from September 2014 through March 2015. This method provided larger spatial and temporal SSC observations than the in situ data could, thus giving better validation data for system-wide numerical models.

To generate an algorithm specific to the Mekong Delta system, we performed

a regression analysis between the in situ SSC values and ratios of the average MSI reflectances. The results show that the blue/red ratio had the best linear fit to the logarithm of SSC if the SSC was $< 0.07 \text{ g L}^{-1}$. The NIR/green ratio had the best linear fit to the logarithm of SSC if the SSC was $> 0.07 \text{ g L}^{-1}$. Thus, we had two different retrieval algorithms, depending on whether the regime was turbid or not. The value of the individual red band proved the best indicator of regime for any given location: if the red band had a reflectance < 0.17 , then the blue/red retrieval algorithm was used; if it was > 0.17 , then the NIR/green was used. Final performance of the combined regression fits against the test data generated a root-mean-square error (RMSE) of 0.034 g L^{-1} for the estimated SSC. The regression model was then applied to the full set of remote-sensing imagery collected during the experiment to generate a time series of spatial maps for SSC across the Mekong Delta from September 2014 through March 2015. The images in Figure 5 show two examples of the spatial distribution for SSC measured using the MODIS-Aqua sensor.

To quantify the remote-sensing estimates, locations within the Song Hau distributary were identified to provide extended spatial and temporal SSC estimates: one upriver before it splits into two subchannels around the island of Cu Lao Dung (identified as location C in the top image of Figure 6), one in each of

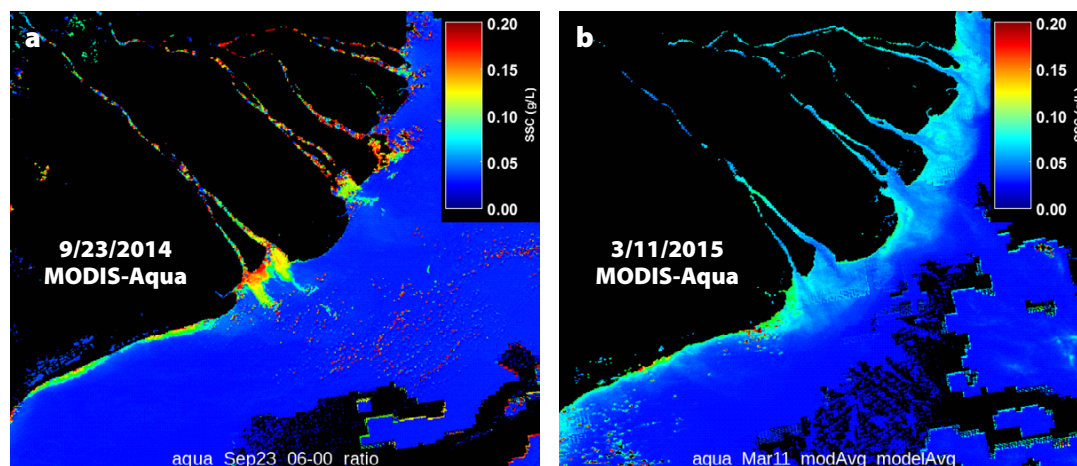


FIGURE 5. Examples of spatial maps of suspended sediment concentrations (SSC) derived from remote-sensing imagery using an empirically derived relationship between the logarithm of SSC and ratios of multi-spectral image bands. Panel (a) shows data derived from the MODIS-Aqua sensor collected on September 23, 2014. Panel (b) shows data derived from the same sensor but on March 11, 2015.

the two subchannels right below the split (B and B'), one in each of the subchannels farther down river (A and A'), and one in each of the subchannel plume regions (P and P'). The four sites within the subchannels were also locations where in situ SSC observations are available. For every remote-sensing image collected from September 2014 through March 2015, the regression model was used to estimate SSC if the region was cloud-free and a spatial average across the river or channel was generated, making sure that no land samples were included.

The temporal sampling of remote-sensing imagery can miss diurnal or episodic sediment events. Thus, the utility of remote-sensing imagery is in generating long-term trends, typically monthly averages that can be used to help interpret in situ observations and validate similarly derived model estimates. Remote sensing can aid in recognition of spatial trends—what is happening along a river coincident with observations at specific locations. It can also help predict temporal

trends—what is happening when the observations are not being made. To estimate spatial trends for the Mekong Delta locations, monthly averages of SSC at each location were calculated for high-flow conditions in September 2014 and low-flow conditions in March 2015 (Figure 6b).

Error bars were generated from the standard deviation of the SSC estimates over the month, and they were consistent with the RMSE values derived from the regression fit (0.037 g L^{-1} for the monthly averages versus 0.034 g L^{-1} for the regression fit). Comparisons to in situ observations at four subchannel locations (A, A', B, B') averaged over their observation times (usually 9–12 hours for 1–2 days) were within the standard deviation of the remote-sensing means as long as there was a temporal overlap between the observations (Figure 6b). There was one case where in situ observations made over nine hours on March 8, 2015, had no coincident remote-sensing imagery and showed large SSC events that

were not captured in the remote-sensing monthly averages, highlighting the issue that the estimates may miss these events. However, the overall trend in the spatial data shows generally higher SSC values during the high-flow season versus the low-flow, and is consistent with in situ observations that during high-flow SSC was 30% lower at location B than A, but during low-flow it was lower at A than B (Nowacki et al., 2015; McLachlan et al., in press).

The remote-sensing estimates also show that during high flow, there is a general increase in SSC moving from upriver (B, B') to the plumes (P, P') that is absent during low flow. If this were due to mixing within the upper water column, it would be consistent with the in situ observations of a salt wedge intrusion that is observed in high-flow conditions, reaching only to location A (Nowacki et al., 2015; McLachlan et al., in press). The salt wedge is not observed during low-flow conditions, consistent with the more uniform remote-sensing SSC estimates along

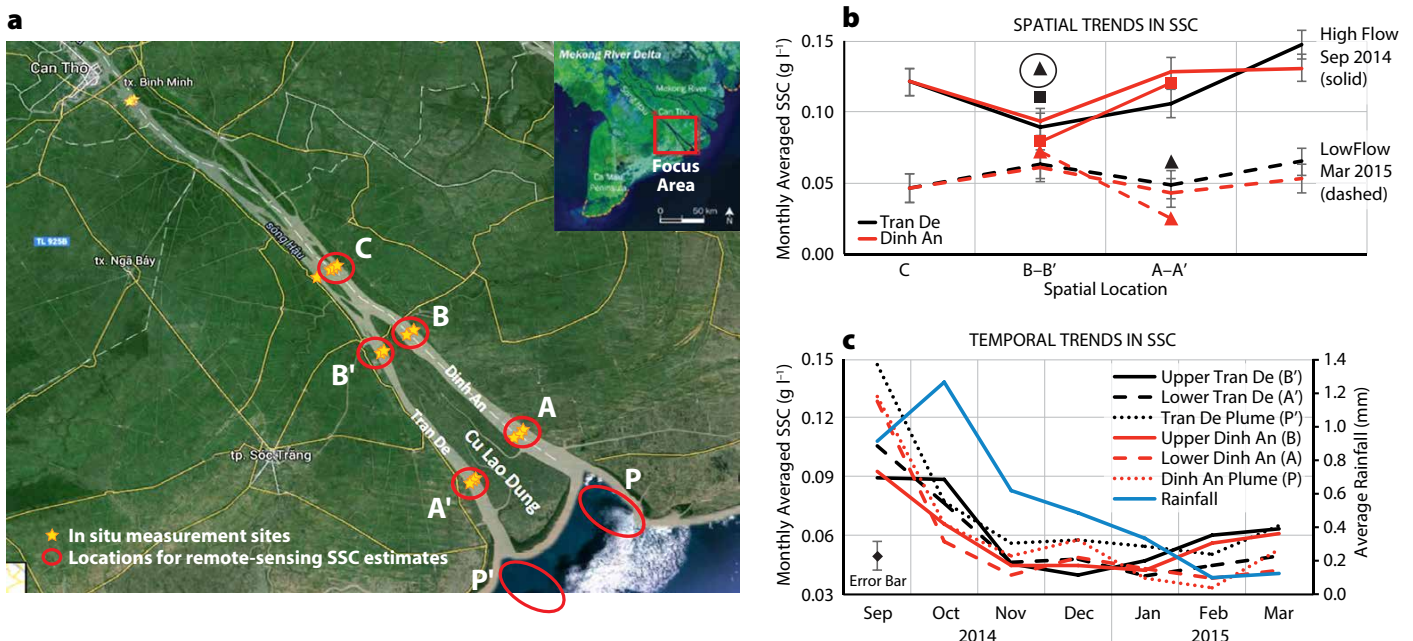


FIGURE 6. Spatial and temporal trends in SSC derived from remote-sensing imagery that can be used to provide context for limited in situ observations or validation data for model estimates. (a) Image showing the locations (indicated by letters) where monthly averages of SSC were generated from remote-sensing imagery. From Wackerman et al. (in press) (b) Spatial trends in SSC from remote-sensing imagery for high-flow conditions during September 2014 (solid lines) and low-flow conditions during March 2015 (dashed lines). Black data are from the Tran De subchannel, and red data are from the Dinh An subchannel. Symbols are averaged in situ observations; squares indicate high-flow and triangles low-flow periods. The circled black triangle denotes an in situ data set collected during a turbid SSC event that was not imaged with any remote-sensing system. (c) Temporal trends in SSC from remote-sensing imagery compared to average rainfall. Black data are from the Tran De subchannel, and red data are from the Dinh An subchannel. Solid lines are for locations B, B', dashed for locations A, A', and dotted lines for plume locations. To keep the plot uncluttered, the error bar for all of the remote-sensing data is shown at bottom left. From Wackerman et al. (in press)

the river during low flow.

Characteristics of the temporal transition from high- to low-flow conditions can be estimated by examining monthly SSC averages from September 2014 to March 2015 (Figure 6c). A decrease in SSC through November 2014 can be seen as the average rainfall decreases to 0.6 mm. Then, the SSC is relatively constant for the remainder of the period, with a noted increase in sediment just when the river splits into the channels (locations B and B') for the lowest rain months of February 2015 and March 2015. Note also that the Tran De plume region consistently has either greater or similar sediment concentrations to the Dinh An plume throughout the time period, with a noted increase in the Tran De over the Dinh An during low rain, low-flow conditions.

The remote-sensing imagery was useful during the Mekong Delta campaign because it provided this extended context for the in situ observations. It supplied SSC trends along the river when the in situ observations were made for only

a limited portion of the river. It also provided SSC trends in time from high- to low-flow conditions, although the in situ observations were made only at the beginning and end of this time period.

Remote-sensing imagery can also give indications of the consequences for sediment distributions. Images of the tidal mud flat region off Cu Lau Dung during similar tide heights show the flat extending farther from shore near the Tran De subchannel. By measuring the extent of the mudflat from images collected at different stages of the tidal cycle, the slope of the mudflat can be estimated along cross-shore transects. This shows that the slope is relatively constant except at the protrusion near the mouth of the Tran De subchannel, where the intertidal topography steepens sharply (Figure 7) and indicates sediment buildup. This is consistent with the remote-sensing observations noted above that show generally increased sediment within the Tran De plume compared to the Dinh An plume. Longer-term trends from these sediment patterns

can also be monitored using the decades-long imagery collected from sensors such as Landsat. Examining imagery from 1989 through 2014 collected during the same months (April and May) we can see that the mangrove/water boundary has grown farther seaward at the southern edge, closest to the Tran De subchannel, than the northern edge, closer to the Dinh An subchannel (Figure 8).

SUMMARY AND DISCUSSION

The coastal zones of the world are highly productive and dynamic ecosystems, with significant human reliance on their natural resources for food, commerce, and recreation.

Demands on these ecosystems have changed over time and have increased coincident with the rapid rise in human habitation of coastal areas. Predictive numerical models are viable tools to advance understanding of the basic governing processes of deltaic and coastal systems, and provide insights on how these natural systems respond to

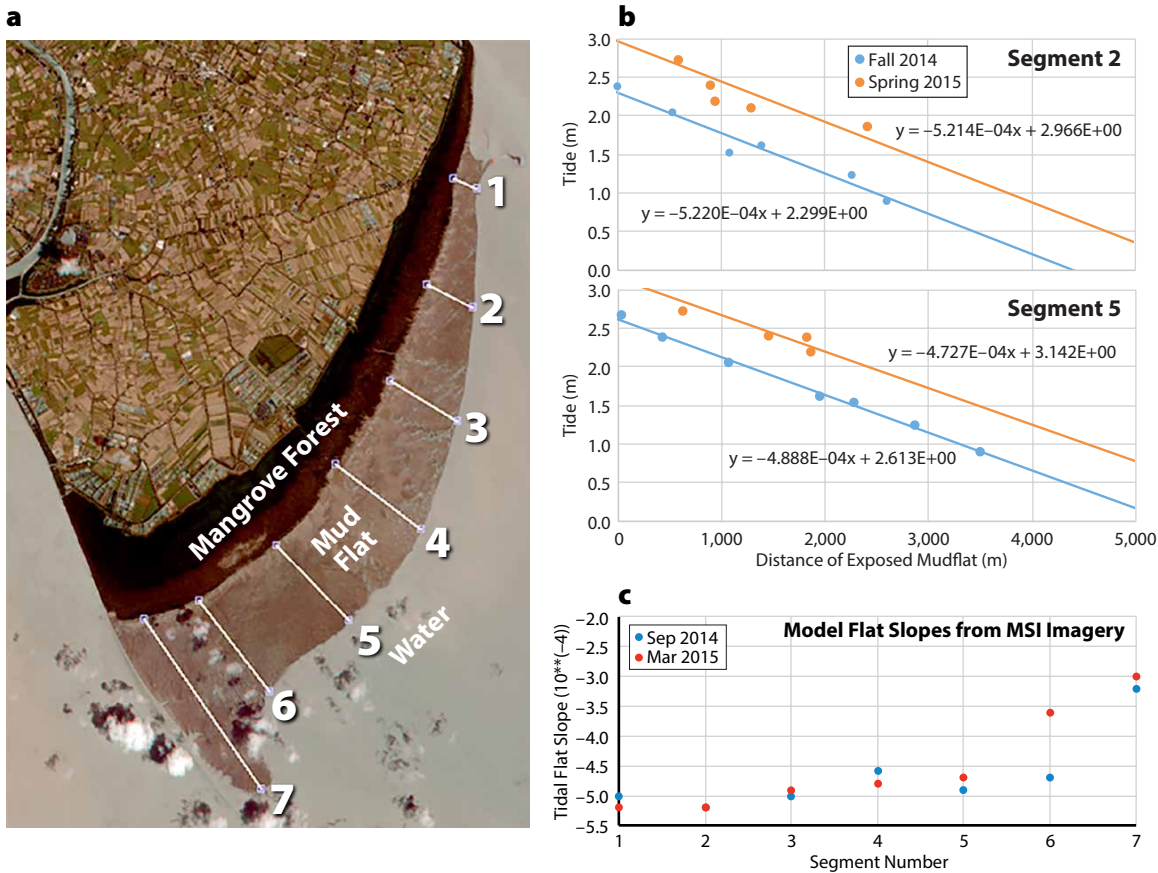


FIGURE 7. Estimation of mud flat slope using a time series of remote-sensing imagery. Panel (a) shows one realization of the mud flat shape, with seven lines indicating the locations where slope was estimated. The extent of the exposed mud flat along these lines was estimated at various tidal heights; (b) the two plots show examples for two of the line segments. Line slopes estimate mud flat-slopes; this is plotted in (c) for each of the line segments, indicating a sharp decrease in slope at the southern end of the island.

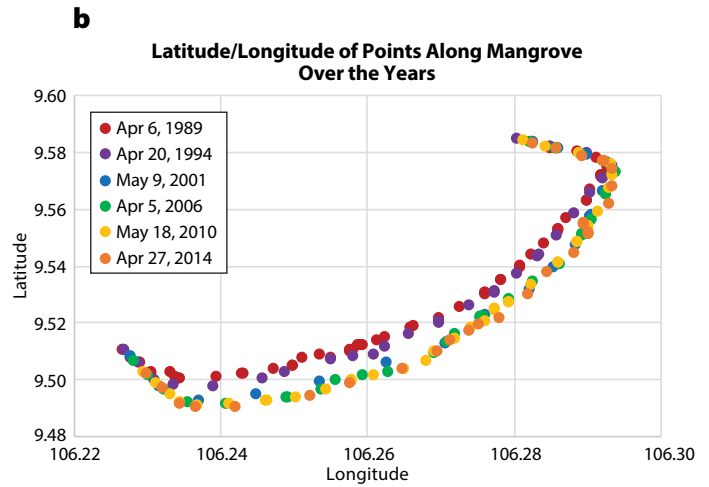



FIGURE 8. Long-term series of Landsat MSI images from April 1989 through April 2014, allowing the growth of the mangrove forest region to be estimated. Six panels (a) show the imagery over this time period. Panel (b) shows the manually extracted mangrove forest edge for each image, indicating larger growth in the southern part of the island.

anthropogenic changes. Numerical models can also be used to assess the effectiveness of restoration and protection strategies intended to ameliorate the effects of sea level rise and storms on coastal ecosystems and human communities. While these predictive tools have been extensively and successfully used for numerous studies and practical applications, advancements and refinements of their capabilities are still needed. Specifically, improving integration of ecologic, morphologic, and hydrologic processes (including their feedbacks) into models is a subject of active research and will result in better numerical representation of these natural systems.

One of the challenges to those applying predictive numerical modeling to large deltaic and coastal systems is the availability of data needed for setup and ground truthing. Remote-sensing techniques provide information and imagery that cover large spatial scales and temporal scales from days to years or even decades. Information that can be extracted from remotely sensed satellite imagery and that can be quite valuable in validating and parameterizing numerical models

includes sediment concentration, chlorophyll, and temperature. These parameters are particularly valuable in regions where access is limited due to expense or availability of logistical support. It should be emphasized that remote-sensing values must be ground truthed through in situ observations to be useful.

In this study, remote-sensing information compared reasonably well against in situ data collected through traditional means. For estimates of SSC, the RMSE between remote-sensing and in situ observations is 0.034 g L^{-1} and the R^2 values are 0.75 for the higher sediment concentration model and 0.69 for the lower concentration model. Further studies and research are needed to enhance the quality of the remote-sensing imagery and the ability of the sensors that collect it to penetrate the water surface, and also to improve the algorithms used to translate remote-sensing imagery to quantities of interest. 

REFERENCES

Aerts, J.C., W.J. Wouter Botzen, K. Emanuel, N. Lin, H. de Moel, and E.O. Michel-Kerjan. 2014. Evaluating flood resilience strategies for coastal megacities. *Science* 344:473–475, <https://doi.org/10.1126/science.1248222>.

Allison, M.A. 1998. Historical changes in the Ganges-Brahmaputra delta front. *Journal of Coastal Research* 14:1,269–1,275.

Allison, M.A., C.R. Demas, B.A. Ebersole, B.A. Kleiss, C.D. Little, E.A. Meselhe, N.J. Powell, T.C. Pratt, and B.M. Vosburg. 2012. A water and sediment budget for the lower Mississippi–Atchafalaya River in flood years 2008–2010: Implications for sediment discharge to the oceans and coastal restoration in Louisiana. *Journal of Hydrology* 432:84–97, <https://doi.org/10.1016/j.jhydrol.2012.02.020>.

Allison, M.A., H.D. Weathers III, and E.A. Meselhe. In press. Bottom morphology in the Song Hau distributary channel, Mekong River Delta, Vietnam. *Continental Shelf Research*, <https://doi.org/10.1016/j.csr.2017.05.010>.

Allison, M.A., and C.F. Neill. 2002. Accumulation rates and stratigraphic character of the modern Atchafalaya River prodelta, Louisiana. *Gulf Coast Association of Geological Societies Transactions* 53:1,031–1,040.

Anthony, E.J., G. Brunier, M. Besset, M. Goichot, P. Dussouillez, and V.L. Nguyen. 2015. Linking rapid erosion of the Mekong River delta to human activities. *Scientific Reports* 5:14745, <https://doi.org/10.1038/srep14745>.

Barua, D.K. 1990. Suspended sediment movement in the estuary of the Ganges-Brahmaputra-Meghna river system. *Marine Geology* 91, 243–253, [https://doi.org/10.1016/0025-3227\(90\)90039-M](https://doi.org/10.1016/0025-3227(90)90039-M).

Bowers, D.G., and C.E. Binding. 2006. The optical properties of mineral suspended particles: A review and synthesis. *Estuarine, Coastal and Shelf Science* 67:219–230, <https://doi.org/10.1016/j.ecss.2005.11.010>.

Bravard, J.P., M. Goichot, and H. Tronchère. 2014. An assessment of sediment-transport processes in the Lower Mekong River based on deposit grain sizes, the CM technique and flow-energy data. *Geomorphology* 207:174–189, <https://doi.org/10.1016/j.geomorph.2013.11.004>.

- Caldwell, R.C., and D.A. Edmonds. 2014. The effects of sediment properties on deltaic processes and morphologies: A numerical modeling study. *Journal of Geophysical Research* 119(5):961–982, <https://doi.org/10.1002/2013JF002965>.
- Carew-Reid, J. 2008. Rapid assessment of the extent and impact of sea level rise in Viet Nam. Climate Change Discussion Paper 1, International Centre for Environmental Management 82.
- Curran, P.J., and E.M.M. Novo. 1988. The relationship between suspended sediment concentration and remotely sensed spectral radiance: A review. *Journal of Coastal Research* 4:351–368.
- Deltares. 2011. Simulation of multi-dimensional hydrodynamic flows and transport phenomena, including sediments. User Manual Delft-3D Flow.
- Dennison, W.C. 2008. Environmental problem solving in coastal ecosystems: A paradigm shift to sustainability. *Estuarine, Coastal and Shelf Science* 77(2):185–196, <https://doi.org/10.1016/j.ecss.2007.09.031>.
- Doxaran, D., J.M. Froidefond, and P. Castaing. 2003. Remote-sensing reflectance of turbid sediment dominated waters: Reduction of sediment type variations and changing illumination conditions effects by use of reflectance ratios. *Applied Optics* 42:2,623–2,634, <https://doi.org/10.1364/AO.42.002623>.
- Doxaran, D., J.M. Froidefond, P. Castaing, and M. Babin. 2009. Dynamics of the turbidity maximum zone in a macrotidal estuary (the Gironde, France): Observations from field and MODIS satellite data. *Estuarine, Coastal and Shelf Science* 81:321–332, <https://doi.org/10.1016/j.ecss.2008.11.013>.
- Doxaran, D., J.M. Froidefond, S. Lavender, and P. Castaing. 2002. Spectral signature of highly turbid waters: Application with SPOT data to quantify suspended particulate matter concentrations. *Remote Sensing of Environment* 81:149–161, [https://doi.org/10.1016/S0034-4257\(01\)00341-8](https://doi.org/10.1016/S0034-4257(01)00341-8).
- Edmonds, D.A., and R.L. Slingerland. 2007. Mechanics of river mouth bar formation: Implications for the morphodynamics of delta distributary networks. *Journal of Geophysical Research* 112, F02034, <https://doi.org/10.1029/2006JF000574>.
- Eidam, E.F., C.A. Nittrouer, A.S. Ogston, D.J. DeMaster, J.P. Liu, T.T. Nguyen, T.N. Nguyen. In press. Dynamic controls on shallow clinoform geometry: Mekong Delta, Vietnam. *Continental Shelf Research*, <https://doi.org/10.1016/j.csr.2017.06.001>.
- Erban, L.E., S.M. Gorelick, and H.A. Zebker. 2014. Groundwater extraction, land subsidence, and sea-level rise in the Mekong Delta, Vietnam. *Environmental Research Letters* 9:84010, <https://doi.org/10.1088/1748-9326/9/8/084010>.
- Ericson, J.P., C.J. Vörösmarty, S.L. Dingman, L.G. Ward, and M. Meybeck. 2006. Effective sea level rise and deltas: Causes of change and human dimension implications. *Global Planet Change* 50:63–82, <https://doi.org/10.1016/j.gloplacha.2005.07.004>.
- Gagliano, S.M., and W.G. McIntire. 1968. *Reports on the Mekong River Delta*. Technical Report #57, Coastal Studies Institute, Louisiana State University, Baton Rouge, 145 pp.
- Gaweesh, A., and E.A. Meselhe. 2016. Evaluation of sediment diversion design attributes and their impact on the capture efficiency. *Journal of Hydraulic Engineering* 142(5), [https://doi.org/10.1061/\(ASCE\)HY:1943-7900.0001114](https://doi.org/10.1061/(ASCE)HY:1943-7900.0001114).
- Giosan, L., J. Syvitski, S. Constantinescu, and J. Day. 2014. Protect the world's deltas. *Nature* 516(7529):31–33, <https://doi.org/10.1038/516031a>.
- Hein, H., B. Hein, and T. Pohlmann. 2013. Recent sediment dynamics in the region of Mekong water influence. *Global Planet Change* 110:183–194, <https://doi.org/10.1016/j.gloplacha.2013.09.008>.
- Holyer, R.J. 1978. Toward universal multispectral suspended sediment algorithms. *Remote Sensing of Environment* 7:323–338, [https://doi.org/10.1016/0034-4257\(78\)90023-8](https://doi.org/10.1016/0034-4257(78)90023-8).
- Hori, K., Y. Saito, Q. Zhao, X. Cheng, P. Wang, Y. Sato, and C. Li. 2001. Sedimentary facies of the tide-dominated paleo-Changjiang (Yangtze) estuary during the last transgression. *Marine Geology* 177(3):331–351, [https://doi.org/10.1016/S0025-3227\(01\)00165-7](https://doi.org/10.1016/S0025-3227(01)00165-7).
- Hori, K., Y. Saito, Q. Zhao, and P. Wang. 2002. Architecture and evolution of the tide dominated Changjiang (Yangtze) River delta, China. *Sedimentary Geology* 146(3):249–264, [https://doi.org/10.1016/S0037-0738\(01\)00122-1](https://doi.org/10.1016/S0037-0738(01)00122-1).
- Jian, J., P.J. Webster, and C.D. Hoyos. 2009. Large-scale controls on Ganges and Brahmaputra river discharge on intraseasonal and seasonal time-scales. *Quarterly Journal of the Royal Meteorological Society* 135(639):353–370, <https://doi.org/10.1002/qj.384>.
- Kilham, N.E., and D. Roberts. 2011. Amazon River time series of surface sediment concentration from MODIS. *International Journal of Remote Sensing* 32:2,659–2,679, <https://doi.org/10.1080/01431161003713044>.
- Kilham, N.E., D. Roberts, and M.B. Singer. 2012. Remote sensing of suspended sediment concentration during turbid flood conditions on the Feather River, California: A modeling approach. *Water Resources Research* 48, W01521, <https://doi.org/10.1029/2011WR010391>.
- Kim, W., D. Mohrig, R. Twilley, C. Paola, and G. Parker. 2009. Is it feasible to build new land in the Mississippi River Delta? *Eos* 90:373–374, <https://doi.org/10.1029/2009EO420001>.
- Kirk, J.T.O. 1994. *Light and Photosynthesis in Aquatic Ecosystems*. Cambridge University Press, Cambridge, 401 pp.
- Kondolf, G.M., G. Annandale, and Z.A.N. Rubin. 2015. Sediment starvation from dams in the Lower Mekong River Basin: Magnitude of the effect and potential mitigation opportunities. E-proceedings 36th International Association of Hydraulic Research World Congress, http://app.iahr2015.info/programma_details/3440.
- Lesser, G.R., J.A. Roelvink, J.A.T.M. Van Kester, and G.S. Stelling. 2004. Development and validation of a three-dimensional morphological model. *Coastal Engineering* 51:883–915, <https://doi.org/10.1016/j.coastaleng.2004.07.014>.
- Long, C.M., and T.M. Pavelsky. 2013. Remote sensing of suspended sediment concentration and hydrological connectivity in a complex wetland environment. *Remote Sensing of Environment* 129:197–209, <https://doi.org/10.1016/j.rse.2012.10.019>.
- Lu, X.X., S. Li, M. Kummur, R. Padawangi, and J.J. Wang. 2014. Observed changes in the water flow at Chiang Saen in the lower Mekong: Impacts of Chinese dams? *Quarterly International* 336:145–157, <https://doi.org/10.1016/j.jqaint.2014.02.006>.
- Manh, N.V., N.V. Dung, N.N. Hung, M. Kummur, B. Merz, and H. Apel. 2015. Future sediment dynamics in the Mekong Delta floodplains: Impacts of hydro-power development, climate change and sea level rise. *Global and Planetary Change* 127:22–33, <https://doi.org/10.1016/j.gloplacha.2015.01.001>.
- McGranahan, G., D. Balk, and B. Andreson. 2007. The rising tide: Assessing the risk of climate change and human settlements in low elevation coastal zones. *Environment and Urbanization* 19(1):17–37, <https://doi.org/10.1177/0956247807076960>.
- McLachlan, R.L., A.S. Ogston, and M.A. Allison. In press. Implications of tidally-varying bed stress and intermittent estuarine stratification on fine-sediment dynamics through the Mekong's tidal river to estuarine reach. *Continental Shelf Research*, <https://doi.org/10.1016/j.csr.2017.07.014>.
- McSweeney, C., G. Lizcano, M. New, and X. Lu. 2010. The UNDP climate change country profiles: Improving the accessibility of observed and projected climate information for studies of climate change in developing countries. *Bulletin of the American Meteorological Society* 91:157–166, <https://doi.org/10.1175/2009BAMS2826.1>.
- Mertes, L.A.K., M.O. Smith, and J.B. Adams. 1993. Estimating suspended sediment concentrations in surface waters of the Amazon River wetlands from Landsat images. *Remote Sensing of Environment* 43:281–301, [https://doi.org/10.1016/0034-4257\(93\)90071-5](https://doi.org/10.1016/0034-4257(93)90071-5).
- Meselhe, E.A., M.M. Baustian, and M.A. Allison, eds. 2015. *Basin Wide Model Development for the Louisiana Coastal Area Mississippi River Hydrodynamic and Delta Management Study*. The Water Institute of the Gulf. Prepared for and funded by the Coastal Protection and Restoration Authority, Baton Rouge, LA, 314 pp.
- Meselhe, E.A., K.M. Sadid, and M.A. Allison. 2016. Riverside morphological response to pulsed sediment diversion. *Geomorphology* 270:184–202, <https://doi.org/10.1016/j.geomorph.2016.07.023>.
- Miller, R.L., C.C. Liu, C.J. Buonassisi, and A.M. Wu. 2011. A multi-sensor approach to examining the distribution of total suspended matter (TSM) in the Albemarle-Pamlico Estuarine System, NC, USA. *Remote Sensing* 3:962–974, <https://doi.org/10.3390/rs3050962>.
- Milliman, J.D., and K.L. Farnsworth. 2013. *River Discharge to the Coastal Ocean: A Global Synthesis*. Cambridge University Press.
- Milliman, J.D., and J.P. Syvitski. 1992. Geomorphic/tectonic control of sediment discharge to the ocean: The importance of small mountainous rivers. *Journal of Geology* 100(5):525–544, <https://doi.org/10.1086/629606>.
- MONRE (Ministry of Natural Resources and Environment). 2009. *Climate Change, Sea Level Rise Scenarios for Vietnam*. Hanoi, 33 pp.
- Munday, J.C., T.T. Alföldi. 1979. LANDSAT test of diffuse reflectance models for aquatic suspended solids measurement. *Remote Sensing of Environment* 8:169–183, [https://doi.org/10.1016/0034-4257\(79\)90015-4](https://doi.org/10.1016/0034-4257(79)90015-4).
- Nittrouer, C.A., D.J. DeMaster, E.F. Eidam, T.T. Nguyen, J.P. Liu, A.S. Ogston, and P.V. Phung. 2017. The Mekong continental shelf: The primary sink for deltaic sediment particles and their passengers. *Oceanography* 30(3):60–70, <https://doi.org/10.5670/oceanog.2017.314>.
- Nowacki, D.J., A.S. Ogston, C.A. Nittrouer, A.T. Fricke, and V.P.D. Tri. 2015. Sediment dynamics in the lower Mekong River: Transition from tidal river to estuary. *Journal of Geophysical Research* 120:6,363–6,383, <https://doi.org/10.1002/2015JC010754>.
- Nguyen, A.D., H.H.G. Savenije, D.N. Pham, and D.T. Tang. 2008. Using salt intrusion measurements to determine the freshwater discharge distribution over the branches of a multi-channel estuary: The Mekong Delta case. *Estuarine, Coastal and Shelf Science* 77:433–445, <https://doi.org/10.1016/j.ecss.2007.10.010>.
- Ogston, A.S., M.A. Allison, J.C. Mullarney, and C.A. Nittrouer. In press. Sediment- and hydro-dynamics of the Mekong Delta: From tidal river to continental shelf. *Continental Shelf Research*.
- Paola, C., R.R. Twilley, D.A. Edmonds, W. Kim, D. Mohrig, G. Parker, E. Viparelli, and V.R. Voller. 2011. Natural processes in delta restoration: Application to the Mississippi Delta. *Annual Review of Marine Science* 3(1):67–91, <https://doi.org/10.1146/annurev-marine-120709-142856>.

Park, E., and E.M. Latrubesse. 2014. Modeling suspended sediment distribution patterns of the Amazon River using MODIS data. *Remote Sensing of Environment* 147:232–242, <https://doi.org/10.1016/j.rse.2014.03.013>.

Pavelsky, T.M., and L.C. Smith. 2009. Remote sensing of suspended sediment concentration, flow velocity, and lake recharge in the Peace-Athabasca Delta, Canada. *Water Resources Research* 45, W11417, <https://doi.org/10.1029/2008WR007424>.

Rabouille, C., D.J. Conley, M.H. Dai, W.J. Cai, C.T.A. Chen, B. Lansard, R. Green, K. Yin, P.J. Harrison, M. Dagg, and B. McKee. 2008. Comparison of hypoxia among four river-dominated ocean margins: The Changjiang (Yangtze), Mississippi, Pearl, and Rhone Rivers. *Continental Shelf Research* 28(12):1,527–1,537, <https://doi.org/10.1016/j.csr.2008.01.020>.

Ritchie, J.C., F.R. Schiebe, and J.R. McHenry. 1976. Remote sensing of suspended sediments in surface waters. *Photogrammetric Engineering and Remote Sensing* 42:1,539–1,545.

Ritchie, J.C., P.V. Zimba, and J.H. Everitt. 2003. Remote sensing techniques to assess water quality. *Photogrammetric Engineering and Remote Sensing* 69(6):695–704.

Smith, J.E., S.J. Bentley, G. Snedden, and C. White. 2015. What role do hurricanes play in sediment delivery to subsiding river deltas? *Scientific Reports* 5:17582, <https://doi.org/10.1038/srep17582>.

Sravanthi, N., I.V. Ramana, A.P. Yunus, M. Ashraf, M.M. Ali, and A.C. Narayana. 2013. An algorithm for estimating suspended sediment concentrations in the coastal waters of India using remotely sensed reflectance and its application to coastal environments. *International Journal of Environmental Research* 7(4):841–850.

Stumpf, R.P., and J.R. Pennock. 1989. Calibration of a general optical equation for remote sensing of suspended sediments in a

moderately turbid estuary. *Journal of Geophysical Research* 94(C10):14,363–14,371, <https://doi.org/10.1029/JC094iC10p14363>.

Sutherland, J., D.J.R. Walstra, T.J. Chesher, L.C. Van Rijn, and H.N. Southgate. 2003. Evaluation of coastal area modelling systems at an estuary mouth. *Coastal Engineering* 51:119–142, <https://doi.org/10.1016/j.coastaleng.2003.12.003>.

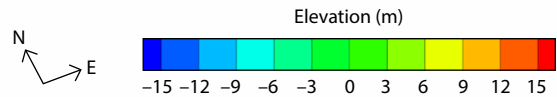
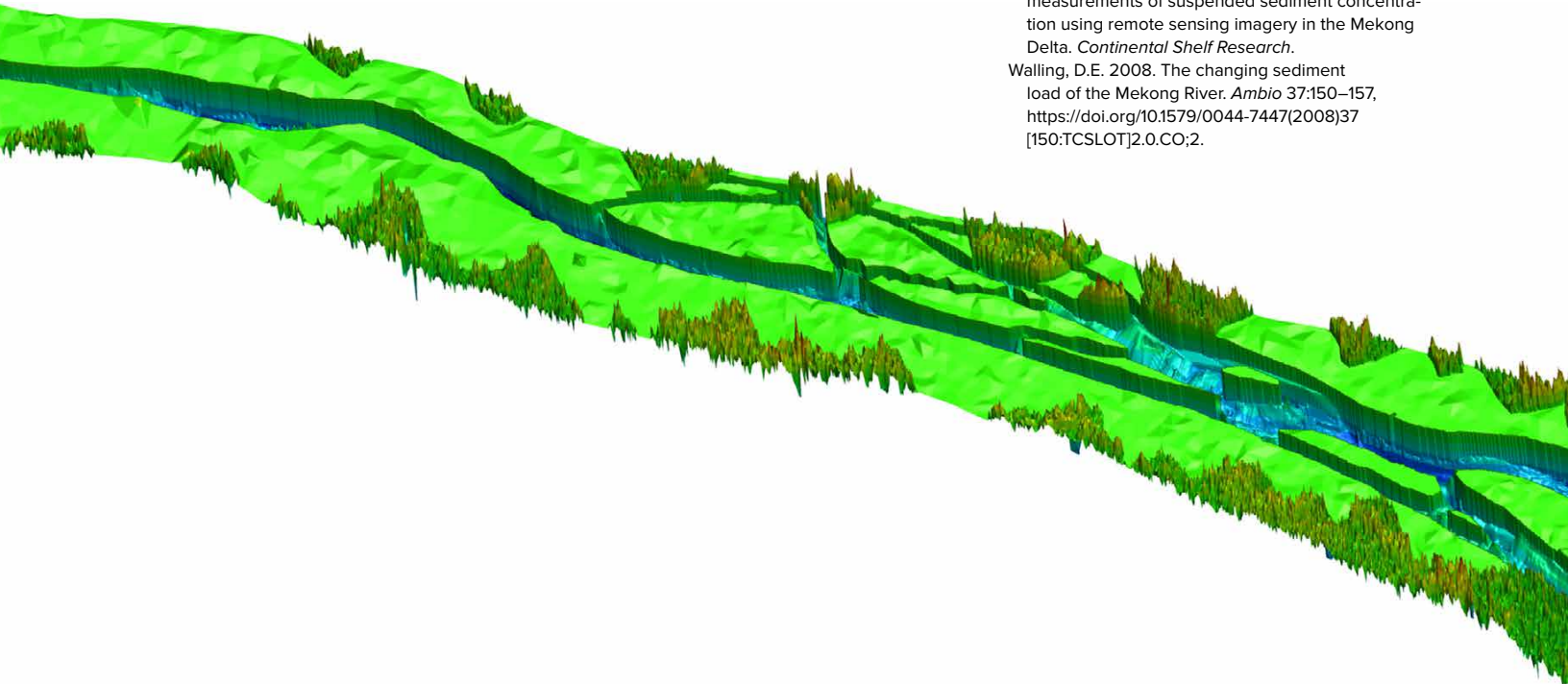
Thanh, V.Q., J. Reyns, C. Wackerman, E.F. Eidam, and D. Roelvink. In press. Modelling suspended sediment dynamics on the subaqueous delta of the Mekong River. *Continental Shelf Research*, <https://doi.org/10.1016/j.csr.2017.07.013>.

Thuy, N.N. 1979. Tides in the Gulf of Thailand and in the coastal regions of the Mekong delta. Symposium, Can-Tho Institute (in Vietnamese).

Vinh, V.D., S. Ouilon, N.V. Thao, and N.N. Tien. 2016. Numerical simulations of suspended sediment dynamics due to seasonal forcing in the Mekong coastal area. *Water* 8(6):255, <https://doi.org/10.3390/w8060255>.

Wackerman, C., A. Hayden, and J. Jonik. In press. Deriving spatial and temporal context for point measurements of suspended sediment concentration using remote sensing imagery in the Mekong Delta. *Continental Shelf Research*.

Walling, D.E. 2008. The changing sediment load of the Mekong River. *Ambio* 37:150–157, [https://doi.org/10.1579/0044-7447\(2008\)37\[150:TCSLOT\]2.0.CO;2](https://doi.org/10.1579/0044-7447(2008)37[150:TCSLOT]2.0.CO;2).



Walsh, J.P., and C.A. Nittrouer. 2009. Understanding fine-grained river-sediment dispersal on continental margins. *Marine Geology* 263(1):34–45, <https://doi.org/10.1016/j.margeo.2009.03.016>.

Wang, J.J., and X.X. Lu. 2010. Estimation of suspended sediment concentrations using Terra MODIS: An example from the lower Yangtze River, China. *Science of the Total Environment* 408:1131–1138, <https://doi.org/10.1016/j.scitotenv.2009.11.057>.

Wolanski, E., N.H. Nhan, and S. Spagnol. 1998. Sediment dynamics during low flow conditions in the Mekong River estuary, Vietnam. *Journal of Coastal Research* 14(2):472–482.

Wright, L.D., and J.M. Coleman. 1974. Mississippi River mouth processes: Effluent dynamics and morphologic development. *Journal of Geology* 82(6):751–778, <https://doi.org/10.1086/628028>.

Wu, H., J. Zhu, and B.H. Choi. 2010. Links between saltwater intrusion and subtidal circulation in the Changjiang Estuary: A model-guided study. *Continental Shelf Research* 30:1891–1905, <https://doi.org/10.1016/j.csr.2010.09.001>.

Xing, F., E.A. Meselhe, M.A. Allison, and H.D. Weathers III. In press. Analysis and numerical modeling of the flow and sand dynamics in the lower Song Hau channel, Mekong Delta. *Continental Shelf Research*.

Xu, K., J. Zhu, and Y. Gu. 2012. Impact of the eastern water diversion from the south to the north project on the saltwater intrusion in the Changjiang Estuary in China. *Acta Oceanologica Sinica* 31:47–58, <https://doi.org/10.1007/s13131-012-0205-0>.

Xue, P., C. Chen, P. Ding, R.C. Beardsley, H. Lin, J. Ge, and Y. Kong. 2009. Saltwater intrusion into the Changjiang River: A model-guided mechanism study. *Journal of Geophysical Research* 114:1–15, <https://doi.org/10.1029/2008JC004831>.

Xue, Z., J.P. Liu, and Q. Ge. 2011. Changes in hydrology and sediment delivery of the Mekong River in the last 50 years: Connection to damming, monsoon, and ENSO. *Earth Surface Processes and Landforms* 36:296–308, <https://doi.org/10.1002/esp.2036>.

Yuill, B.T., A. Gaweesh, M.A. Allison, and E.A. Meselhe. 2015. Morphodynamic evolution of a Lower Mississippi River channel bar after sand mining. *Earth Surface Processes and Landforms* 41(4):526–542, <https://doi.org/10.1002/esp.3846>.

Yuill, B.T., A.K. Khadka, J. Pereira, M.A. Allison, and E.A. Meselhe. 2016. Morphodynamics of the erosional phase of crevasse-splay evolution and implications for river sediment diversion function. *Geomorphology* 259:12–29, <https://doi.org/10.1016/j.geomorph.2016.02.005>.

Zhu, Z., and C.E. Woodcock. 2012. Object-based cloud and cloud shadow detection in Landsat imagery. *Remote Sensing of Environment* 118:83–94, <https://doi.org/10.1016/j.rse.2011.10.028>.

ACKNOWLEDGMENTS

This research was funded by Office of Naval Research (ONR, grant numbers N00014-15-1-2011, N00014-13-1-0127, N00014-13-1-0781) as a part of the project “Coupled Process Studies and Numerical Simulations of Channel Sand Dynamics in Tide-Dominated River Channels: A Mekong Delta Case Study,” and as part of the Mekong Delta Directed Research Initiative (N00014-13-C-0128,

N00014-16-C-3013). The authors appreciate Vo Luong, Hong Phuoc, Richard Nguyen, and all the Vietnamese colleagues who participated in the efforts to make the research program possible.

AUTHORS

Ehab Meselhe (emeselhe@thewaterinstitute.org) is Vice President for Science & Engineering, The Water Institute of the Gulf, Baton Rouge, LA, USA. **Dano Roelvink** is Professor, Institute for Water Education, UNESCO-IHE, Delft, The Netherlands. **Christopher Wackerman** is Senior Manager of Research Programs, MDA Information Systems LLC, Ypsilanti, MI, USA. **Fei Xing** is Postdoctoral Fellow, The Water Institute of the Gulf, Baton Rouge, LA, USA. **Vo Quoc Thanh** is PhD Fellow, Can Tho University, Can Tho, Vietnam.

ARTICLE CITATION

Meselhe, E., D. Roelvink, C. Wackerman, F. Xing, and V.Q. Thanh. 2017. Modeling the process response of coastal and deltaic systems to human and global changes: Focus on the Mekong system. *Oceanography* 30(3):84–97, <https://doi.org/10.5670/oceanog.2017.317>.

